

## 2. Principles of Optical Spectroscopy

The term ‘spectroscopy’ is applied to a vast range of experimental techniques in which one or more of the measurable properties of a system are resolved into a range of energies, wavelength, or other appropriate unit. Examples of the measured property of the system might be the energy of electrons emitted from a material’s surface, the time delay between light being absorbed and then re-emitted in the bulk of a sample, or the mass to charge ratio of ions. This work is concerned with optical spectroscopic techniques suitable for remote analysis of liquid analytes via optical-fibres.

In this chapter the techniques of optical absorption and emission spectroscopy, which are the most appropriate techniques to this goal, are described; the mechanisms of elastic scattering and Fresnel reflection are discussed for their relevance to cell design and as possible sources of optical interference; then the principles of Fourier transform and grating spectrometers, used to measure optical spectra, are described.

### 2.1. Absorption Measurements by Transmission

The most common form of optical spectroscopy is absorption (or transmission) spectroscopy, which is a measure of the amount of light absorbed by (or transmitted through) a sample over a range of optical frequencies. In order of increasing photon energy, the mechanisms for the absorption may be rotational or vibrational transitions of a molecule (in the microwave to IR), overtones of these (IR to visible), or electronic transitions in atoms or molecules (in the visible to UV region).

Whatever the physical basis of the absorption, the experimentally measured parameters are related via the Beer-Lambert law:

$$A = \log_{10} \left( \frac{I_0}{I} \right) = \epsilon(\nu)cl \quad (2.1)$$

According to the expression above, the absorbance  $A$  is proportional to the concentration of the analyte  $c$  and the path length through the sample  $l$  (quantitative information), and the molar absorption coefficient  $\epsilon$  is a function of the optical frequency  $\nu$  (qualitative information).  $I_0$  is the intensity of a beam of collimated light before it enters the medium, and  $I$  is its intensity after it has travelled a length  $l$ . While  $A$  is parameter that is directly measured, in most theoretical

treatments of underlying physics it is more convenient to work with the parameter  $\alpha$ , which is expressed in equation 2.2.

$$\alpha = \frac{\ln(10) \cdot A}{l} \quad (2.2)$$

The basis of most absorption measurements is implicit in equation 2.1; a collimated monochromatic beam of light is transmitted through an absorbing sample, and its intensity is referenced to that of a beam of light that did not pass through the sample. The instruments which make these measurements are called spectrophotometers, and sample holders are available to make measurements over a wide range of absorbance, such as very thin cells for highly absorbing liquids, or long path-length cells for measurements of gases or weakly absorbing liquids. Often the path of the light is folded through the cell, using mirrors or prisms, so that the beam of light makes multiple passes through a small cell.

### 2.1.1. Limitations of absorption measurements

Absorption spectroscopy as a means of quantitative spectroscopic identification may be limited by a number of factors<sup>[35]</sup>. At high concentration, the linear relationship of the Beer-Lambert law breaks down because solute-solute interactions become significant. This can usually be compensated for by calibrating the solution absorbance against reference solutions of known concentration.

Sampling problems are encountered for samples of very high absorbance if insufficient light is transmitted through the sample to make an accurate measurement. In such cases very thin transmission cells are used, or techniques such as *evanescent wave spectroscopy*, where light is removed from the evanescent field of light undergoing total internal reflection (hence the alternative name for the technique of *attenuated total-internal reflection*)<sup>[34]</sup>.

In the visible and near infra-red region (the most convenient part of the spectrum for study over optical fibres) absorption is due to broad, and often weak, overtones of molecular vibrations. If these overlap with strong absorption bands of the solvent, then often no useful information can be deduced. Water is particularly bad as a solvent in this respect, with many broad overtones extending into the visible spectrum.

Conversely, if the solute absorbance is very low, the task of measuring very low concentration solutions is hampered by the problem of measuring a small differences in transmission between

the solution, and the solvent by itself. Shot noise in the collected light will limit such measurements.

## 2.2. Emission Techniques

### 2.2.1. Fluorescent emission

The process of fluorescence in a compound involves the photon-induced excitation of electrons to higher energy levels (*ie* an absorption process), followed by their spontaneous return to a lower energy level, with consequential re-emission of a photon.

The re-emitted photon usually has a lower energy than the incident photon, as energy is often lost by phonon excitation processes (loss of energy to molecular vibrations). The lower energy emission band is called a Stokes band. A band with higher energy than the incident beam is called an anti-Stokes band.

Many aromatic compounds exhibit fluorescence when excited by UV light, but there are also some compounds and materials (*eg* certain organic dyes) having high fluorescence efficiency of optical re-emission when excited by less energetic photons (at other, longer wavelengths). The conversion efficiency is often expressed as a percentage, known as the quantum efficiency  $\eta$ , which is the percentage of the number of absorbed incident photons which result in re-emitted fluorescent photons.

$$\eta = \frac{\text{No. of fluorescent photons}}{\text{No. of absorbed photons}} \times 100\% \quad (2.3)$$

It is essential to effectively separate the desired fluorescent light from the scattered incident light. Fortunately, this problem is assisted by the difference in wavelength arising from the inelastic nature of the fluorescence process. Therefore it is only necessary to provide effective optical filters to remove the incident light from the detected fluorescence signal. If several fluorescent compounds are present, each having different fluorescent wavelengths, they may be detected independently using wavelength-selective bandpass filters or a grating spectrometer with a focal-plane detector array.

### 2.2.1.1. Time resolved fluorescence

This technique takes advantage of the statistical nature of the fluorescence processes. If a large number of molecules are excited by a short pulse of light to the same excited state, and then begin to fall back to their ground state, then

$$I = I_0 \exp(-t/\tau) \quad (2.4)$$

where the fluorescent light intensity  $I$  decays exponentially with the time  $t$  after optical excitation.  $I_0$  is the peak intensity and  $\tau$  the fluorescent lifetime.

In order to measure  $\tau$ , two basic methods are used. The first (time-domain analysis) involves measuring the decay function, following short-pulse optical excitation, and computing the value of  $\tau$  from this function. The second (frequency-domain analysis) uses a source with a sinusoidally-modulated incident light intensity. Either the frequency variation of the fluorescent light intensity as the modulation frequency is varied, or the phase delay between fluorescence and excitation signals (both of which are related to the value of  $\tau$ ) can be monitored. Because of the weak received signal, the frequency-domain methods usually use a coherent electronic detector based on a mixer circuit. This recovers the desired frequency component in the detected signals corresponding to the original sinusoidal modulation signal. If there are compounds in the analyte having distinctly different fluorescent lifetimes, they may be separated using either of the above time-resolved techniques. Also, the time-resolved techniques are complementary to any method of separation of signals in the wavelength domain.

A more typical fluorescent process consists of the excitation of an electron, its non-radiative decay to an intermediate level and subsequent radiative transition back to the ground state. In this case the non-radiative decay is also described by an exponential decay, with its own characteristic time constant. As long as the non-radiative time constant is much shorter than the radiative time constant (as it usually is) equation 2.4 remains valid.

### 2.2.1.2. Limitations of fluorescent spectroscopy

One of the primary problems of fluorescence spectroscopy is the non-linear variation with concentration at high levels of analyte, *ie* when absorption of the incident light becomes large. This causes a reduction in the fluorescent signal for two reasons. Firstly, it reduces the mean optical excitation level in the sample and secondly, at high absorption levels, causes all the absorption to take place close to the point of entry of light into the sample. (In the latter case, efficiency of light collection may be less, due to geometric effects of the measurement apparatus).

Other problems can occur, due to a strong dependence of the fluorescent signals on a variety of environmental parameters. Oxygen usually quenches (*ie* reduces) fluorescence. The pH of a solution, its temperature and any impurities can all influence the fluorescence lifetime and intensity. In addition, many fluorescent materials can become bleached during light absorption. This *photo-bleaching* might be reversible if it is merely due to a long fluorescent lifetime (saturation behaviour); if it is due to a non-reversible photo-chemical reaction it may gradually cause permanent depletion of the fluorophore. As expected, photo-bleaching is most serious at high illumination levels, but unfortunately intense sources are often required for trace analysis.

### 2.2.2. Raman scattering

In this section a brief description of the origin of the Raman effect in gases and liquids is presented, with the important predictions of semi-classical and quantum descriptions of the phenomenon of Raman scattering.

### 2.2.3. Review of the polarizability theory of Raman scattering

Predicted by Adolf Smekal in 1923 and first observed in 1928 by Sir Chandrasekhara Venkata Raman (who was at the time unaware of Smekal's prediction), the spontaneous Raman effect is the basis of an active branch of analytical spectroscopy. In a modern Raman experiment, laser light is shone into a sample and the wavelength spectrum of the scattered light is analysed. The molecular vibrational frequencies may then be deduced from the wavelength shifts acquired by the inelastically scattered light. Different molecules impart their own characteristic spectra of wavelength shifts, from which useful information on the molecules structure may be deduced. Quantitative information for compounds in solution may be derived from the intensity of the inelastically scattered light.

### 2.2.4. Stokes and anti-Stokes lines

The electric dipole moment (vector)  $\underline{\mu}$  induced in a molecule by an externally applied electric field,  $\underline{E}$ , is

$$\underline{\mu} = \underline{\alpha} \cdot \underline{E}. \quad (2.5)$$

For light plane polarised along an arbitrary  $x$ , axis the electric field vector of the incident radiation is given by

$$\underline{E} = E_{0,x} \cdot \sin(\omega t). \quad (2.6)$$

The molecular polarizability  $\underline{\alpha}$  is a tensor quantity. The tensor matrix (equation 2.7) is symmetric about its major axis, and so contains only six independent elements.

$$\underline{\alpha} = \begin{pmatrix} \alpha_{xx} & \alpha_{xy} & \alpha_{xz} \\ \alpha_{yx} & \alpha_{yy} & \alpha_{yz} \\ \alpha_{zx} & \alpha_{zy} & \alpha_{zz} \end{pmatrix} \quad (2.7)$$

If, for illustration, a hypothetical molecule with an isotropic polarizability is considered, only the elements on the major diagonal are non-zero. If the molecule is vibrating with an angular frequency  $\omega_{\text{vib}}$ , and the polarizability is a function of the separation of the nuclei, such that

$$\alpha_{xx} = \alpha_{xx,\text{eq}} + \alpha'_{xx,\text{eq}} \cdot \sin(\omega_{\text{vib}} t) \quad (2.8)$$

where the 'eq' subscript indicates the equilibrium value, and the prime indicates the first differential with respect to the deviation from equilibrium separation. Then plane polarized radiation incident on the molecule induces an electric dipole  $\underline{\mu}$ , which from equation 2.12 written in component form is

$$\begin{aligned} \mu_x &= (\alpha_{xx,\text{eq}} + \alpha'_{xx,\text{eq}} \cdot \sin(\omega_{\text{vib}} t)) E_x \cdot \sin(\omega t) \\ \mu_x &= \alpha_{xx,\text{eq}} E_x \cdot \sin(\omega t) + \frac{1}{2} \alpha'_{xx,\text{eq}} E_x \left( \cos((\omega - \omega_{\text{vib}})t) - \cos((\omega + \omega_{\text{vib}})t) \right) \end{aligned} \quad (2.9)$$

The intensity of radiation emitted from such a dipole is proportional to the change in electric field (dipole moment) squared, and the oscillation of the electric dipole moment contains components (side-bands) with angular frequencies  $\omega - \omega_{\text{vib}}$  and  $\omega + \omega_{\text{vib}}$ . Quantum mechanics shows that these frequencies may take only discrete values, determined by the mass of the atoms in the molecule and the nature of the chemical bonds between the atoms. The bands of lower frequency scattered light are referred to as *Stokes lines*, and the bands at a higher frequency (and hence higher energy) than the exciting light are termed *anti-Stokes lines*<sup>[35]</sup>.

Also apparent from equation 2.9 is that the intensity of radiated Raman light is determined by the square of the differential polarizability  $\alpha'_{\text{eq}}$ , and will not be observed at all if the vibration does not induce a change in the polarizability. Often physical intuition is sufficient to predict which

vibrations of a simple molecule are likely to be Raman active. More rigorously these can be determined by group theory<sup>[35]</sup>. Equation 2.9 does not describe the relative intensities of the Stokes and anti-Stokes bands, which is quantum mechanical in origin (section 2.2.8).

### 2.2.5. Wavenumber (spectroscopist's) units, $\text{cm}^{-1}$

Whereas the wavelength of light,  $\lambda$ , is the natural parameter to use when describing the optics of a system, it is the energy difference,  $E_{\text{tr}}$ , between the incident light and the collected light that is of direct relevance in spectroscopy. This energy difference is normally quoted either as the difference in frequency between the incident and scattered photons (*ie*  $E_{\text{tr}}/h$ , where  $h$  is Planck's constant), or as a wavenumber<sup>[35]</sup> ( $E_{\text{tr}}/hc$ , where  $c$  is the speed of light). In Raman spectroscopy the traditionally accepted units of wavenumber are  $\text{cm}^{-1}$ . Molecular vibrational frequencies are also traditionally quoted in  $\text{cm}^{-1}$ , and to convert a frequency  $\nu$  in Hertz to a frequency in wavenumbers  $\bar{\nu}$ ;  $\bar{\nu}=\nu/c$ , where  $c$  is the speed of light.

It should also be noted that, because  $\lambda$  and  $\sigma$  are not linearly related, when rescaling a plot of intensity *vs* wavelength to one of intensity *vs* frequency shift (or *vice versa*), a correction should be applied to the intensity across the graph, so that the integrated area (which represents energy) under each peak remains constant. Analogous to changing the variable in an integration<sup>[36]</sup>, to accurately represent a measurement in constant divisions of the variable  $u$  on a graph against the variable  $\nu$  multiply the measured values of  $u$  by  $du/d\nu$ . (Another example of this is the Plank radiation curve, which is often plotted against frequency and wavelength<sup>[37]</sup>).

### 2.2.6. Frequency dependence of scattered light intensity

Any light (below the frequency of the electronic resonances) may be used to excite a Raman spectrum. The scattered radiation is essentially that of an oscillating electric dipole<sup>[38]</sup>, the dipole-moment of which is given by equation 2.9. The intensity  $I$  of radiation at a frequency  $\nu$  emitted from such a dipole can be shown to obey

$$I \propto \nu^4. \quad (2.10)$$

### 2.2.7. Depolarization ratio, $\rho_p$

In a liquid, molecules are orientated at random to one-another, and the scattering from such a sample corresponds to the average over all molecular orientations. The results are expressible in

terms of two quantities associated with the tensor  $\underline{\alpha}$  (equation 2.7), the mean value  $\bar{\alpha}$  and the anisotropy  $\gamma$ .

$$\bar{\alpha} = \frac{1}{3}(\alpha_{xx} + \alpha_{yy} + \alpha_{zz})$$

$$\gamma^2 = \frac{1}{2} \left( (\alpha_{xx} - \alpha_{yy})^2 + (\alpha_{yy} - \alpha_{zz})^2 + (\alpha_{zz} - \alpha_{xx})^2 + 6(\alpha_{xy}^2 + \alpha_{yz}^2 + \alpha_{zx}^2) \right) \quad (2.11)$$

For the case where the polarizability is not isotropic,  $\gamma$  is non-zero, and linearly polarized radiation is *depolarised* to some extent after scattering. The depolarization ratio<sup>[39]</sup> (for polarized incident light)  $\rho_p$  may be derived from  $\bar{\alpha}$  and  $\gamma$ ,

$$\rho_p = \frac{I_x}{I_z} = \frac{3\gamma^2}{45\bar{\alpha}^2 + 4\gamma^2}. \quad (2.12)$$

In equation 2.12  $I_y$  and  $I_z$  are the measured intensities of light polarized parallel to the  $x$  and  $z$  axes respectively, measured at  $90^\circ$  to the direction of the incident light, which is polarized parallel to the  $z$  axis.

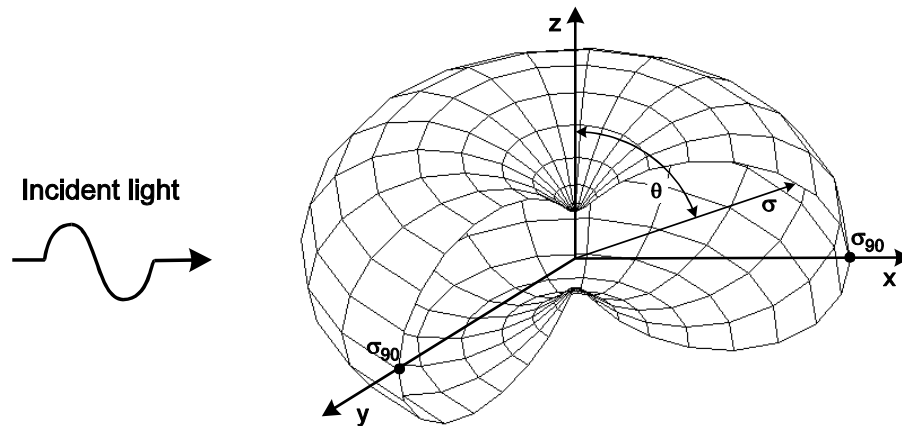


**Figure 2.1** A section from a diagram showing the relative intensity of scattered radiation vs scattering angle, in a liquid of depolarization ratio,  $\rho_p = 0.17$ .

The surface in figure 2.1 shows the intensity distribution of Raman scattered light in water. It is calculated from equation 2.13 (modified from Marshall<sup>[40]</sup> to take into account all polarisations of scattered light and standard spherical coordinates)

$$\sigma = \sigma_{90} \cdot \left( (1 - \rho_p) \sin^2(\theta) + \rho_p \right) \quad (2.13)$$

where  $\sigma$  represents the differential scattering cross section integrated over all molecular orientations and  $\sigma_{90}$  is the light scattered at  $90^\circ$  by one molecule.

The units of  $\sigma$  are  $\text{sr}^{-1}$  (reciprocal steradians).

### 2.2.8. Review of the quantum theory of spontaneous Raman scattering

While the classical polarizability theory of section 2.2.3 does account for the inelastically scattered Raman spectra of molecules, it can not explain even qualitatively why the spectra are manifest as a series of discrete bands. This is the realm of quantum mechanics<sup>[41]</sup>, and some relevant results are presented here with the selection rules which determine which vibrational transitions are allowed, and hence are observed in a Raman spectrum.

### 2.2.9. The molecular potential well and its allowed states

The qualitative form of the potential well between two nuclei, for instance in a diatomic molecule, is shown in figure 2.2<sup>[35]</sup>. The exact form of this curve is generally not known, but as can be seen from the figure, the textbook problem of the parabolic potential is a reasonable approximation for the lower energy part of the curve.

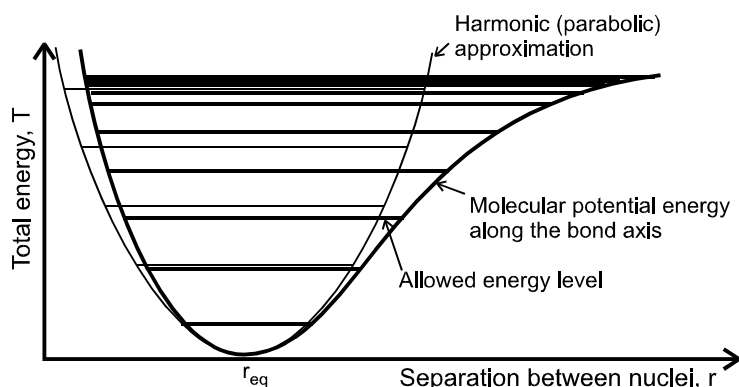


**Figure 2.2** The general form of the internuclear potential along a bond axis, and a parabolic well as assumed in the harmonic approximation, and the quantum mechanically allowed energies.

The properties of systems governed by a parabolic potential are well covered in any undergraduate physics compendium<sup>[42]</sup>. Classically, a harmonic oscillator will vibrate at the same frequency regardless of how much energy is stored in its vibrational motion. The quantum mechanical analogue of this behaviour is that the allowed energy levels that the system may occupy are equally spaced in energy as shown in figure 2.2. The allowed energy levels  $E_V$  that a harmonic oscillator may take are

$$E_V = h\nu(1/2 + V) \quad V = \pm 0, 1, 2, \dots \quad (2.14)$$

where  $V$  is the vibrational quantum number and  $\nu$  is the (classical) frequency of vibration.

Typical molecular vibrational frequencies studied in a Raman experiment are between  $1.5 \times 10^{13}$  Hz and  $1.35 \times 10^{14}$  Hz, corresponding to energy levels spaced, in the harmonic approximation, by  $1 \times 10^{-20}$  J to  $9 \times 10^{-20}$  J. Transitions between these levels correspond to the

energy (and frequency) of IR photons and this is the basis of IR absorption spectroscopy, where photons of energy corresponding to the difference between the energy levels may be absorbed. The interaction between molecule and photon is different for Raman scattering: in this case the photon is not absorbed, but forms a short lived ( $\sim 10^{-13}$  sec) virtual state with the molecule. Effectively the entire ladder of allowed energy states is raised by the energy of the photon. When a virtual state decays, the molecule does not necessarily return to its original energy state (figure 2.3).

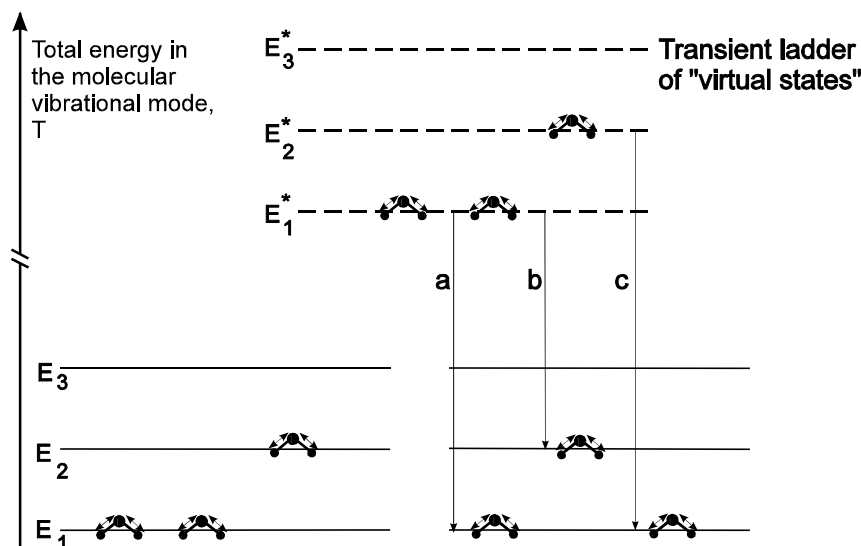


**Figure 2.3** Three molecules and their vibrational states throughout a scattering process (a)  $\Delta V=0$ , Rayleigh scattering (b) Stokes scattering,  $\Delta V=1$  (c) Anti-Stokes scattering,  $\Delta V=-1$ .

The population of the Energy levels  $E_1$ ,  $E_2$ , etc, are governed by a Bose-Einstein distribution<sup>[43]</sup>, and at room temperature the population of levels above the ground state decreases rapidly, which accounts for the much weaker intensity of the anti-Stokes bands in a Raman spectrum.

### 2.2.10. Quantum mechanical selection rules

The probability of transition  $\underline{R}_v$ <sup>[35]</sup> between two eigenstates of a vibrating molecule is given by

$$\underline{R}_v = E_x \int \psi_{v'}^* \underline{\alpha} \psi_{v''} dx \tag{2.15}$$

where  $x$  is the internuclear displacement from equilibrium. If  $\underline{\alpha}$  is expanded to a Taylor series, equation 2.15 can be rewritten as

$$\underline{R}_v = \underline{\alpha}_{eq} \int \psi_{v'}^* \psi_{v''} dx + \frac{d\underline{\alpha}}{dx}_{eq} \int \psi_{v'}^* x \psi_{v''} dx + \frac{1}{2!} \frac{d^2\underline{\alpha}}{dx^2}_{eq} \int \psi_{v'}^* x^2 \psi_{v''} dx + \dots \tag{2.16}$$

where  $\underline{\alpha}_{eq}$  and the subsequent derivatives are the values at mechanical equilibrium. Because  $\psi_{v'}$  and  $\psi_{v''}$  are eigenfunctions of the same Hamiltonian, the first integral in equation 2.16 must be

zero, unless  $V' = V''$  which corresponds to elastic (Rayleigh) scattering of the photon. The integral of the second term can be shown to be finite only when  $V' - V'' = \pm 1$  (for the parabolic potential well approximation), which may be written as in equation 2.17.

$$\Delta V = \pm 1 \quad (2.17)$$

The higher terms in equation 2.16 decrease rapidly due to the factorial prefactor.

Raman scattering intensity is proportional to  $(\underline{R}_v)^2$ , and so again, the intensity of the inelastically scattered Raman light is proportional to the first differential of the polarizability squared (as in section 2.2.4).

### 2.2.11. Anharmonic effects

Two types of anharmonicity may be apparent in a vibrational spectroscopy measurement: *mechanical anharmonicity* is anharmonicity in the inter-nuclear potential (*ie* a deviation from the parabola of figure 2.2); *electrical anharmonicity*, arises from the differential polarizability  $\underline{\alpha}'$  being a function of position (other than a constant). The result of both these deviations from the theory presented above is a relaxation of the vibrational selection rule of equation 2.17 (*ie* the third, and subsequent, terms in equation 2.16 become significant), allowing transitions between any two vibrational levels, so called *overtones*.

The deviation of the molecular potential well from the parabolic approximation becomes more pronounced as the amplitude of a vibration moves the constituent atoms further from their equilibrium positions (figure 2.2). This results in the decrease in the energy level spacing, towards a continuum, so that transitions that are allowed by equation 2.17, but starting from different energy levels, will release different energies (while the parabolic approximation predicts that any transition between adjacent energy levels is equivalent). At the temperatures of concern in this work, only the lower vibrational energy levels are occupied.

In this work the probability of transitions due to anharmonic effects is low, and has been ignored.

### 2.2.12. Rules of thumb in Raman spectroscopy

Only those vibrations which result in a change in the polarizability of the molecule will scatter light inelastically, and are said to be Raman active. Diatomic molecules always have Raman

active vibrations, and in general if a vibration preserves all of the symmetry elements of a molecule then the vibration will be Raman active.

Vibrations which result in particularly large changes in polarizability produce more intense Raman signals. These are often vibrations of atoms bonded by  $\pi$ -bonds, or large resonance bonds (eg benzene). Stronger Raman bands are normally expected from bonds between elements in the second and subsequent rows of the periodic table (as they have more electrons), cyclical molecules (such as benzene) and hydrogenic molecules (those containing hydrogen).

Liquids with large intermolecular interactions (such as those due to hydrogen bonding, in the case of water) will have broad bands, as the frequency at which a molecule vibrates will be affected by the particular orientation of the molecule with respect to its neighbours.

The intensity of the scattered radiation is proportional to the fourth power of the incident photon frequency, and has a spatial distribution as shown in figure 2.1. Typically a proportion of order  $10^{-2}$  of the incident photons will be scattered elastically, and a fraction of only  $10^{-4}$  of this shifted in wavelength. As higher frequency radiation is used to increase Rayleigh and Raman scattering a compromise arises for the best wavelength for Raman analysis, eventually the photon energies will correspond to electronic transitions within the sample. A sufficiently high energy photon may be absorbed by the molecule (rather than scattered) and then re-emitted as fluorescence (after a characteristic fluorescence lifetime much greater than the  $10^{-13}$  seconds of a scattering event). Fluorescence bands are spectrally-broad and typically four to six orders of magnitude stronger than the weak Raman lines<sup>[44]</sup>. Fluorescence is not normally a problem with infrared excitation, but becomes significant with radiation in the visible to ultra-violet region. Except for rare two photon absorption events, fluorescence is usually of a lower energy than the radiation which excites it, and so is seldom a problem in the study of the even weaker anti-Stokes bands.

### 2.2.13. Absolute intensity measurements

Making absolute determinations of the amount of light scattered into the optics of a spectrometer or interferometer is difficult. The small intensity of the Raman scattered light, and the precautions taken to reject any inelastically scattered light, both necessitate careful calibration with a reference radiance standard. In practice, if the absolute value of the scattered radiance must be found, the intensity of the spectrum is compared with that of a secondary standard<sup>[45][46][47]</sup>.

Absolute Raman scattering cross sections found in this way are tabulated for some gases and organic liquids in Weber<sup>[45]</sup>. More recent measurements of liquids (organic and halide ion solutions) have been made by Eysel<sup>[46][48]</sup> and the scattering cross section of water is measured and discussed by Marshall<sup>[40]</sup>. Fischer<sup>[49]</sup> and co workers have demonstrated for aqueous solutions at concentrations below 1 M, the background Raman spectrum due to the water is unchanged in shape, although its intensity may decrease slightly.

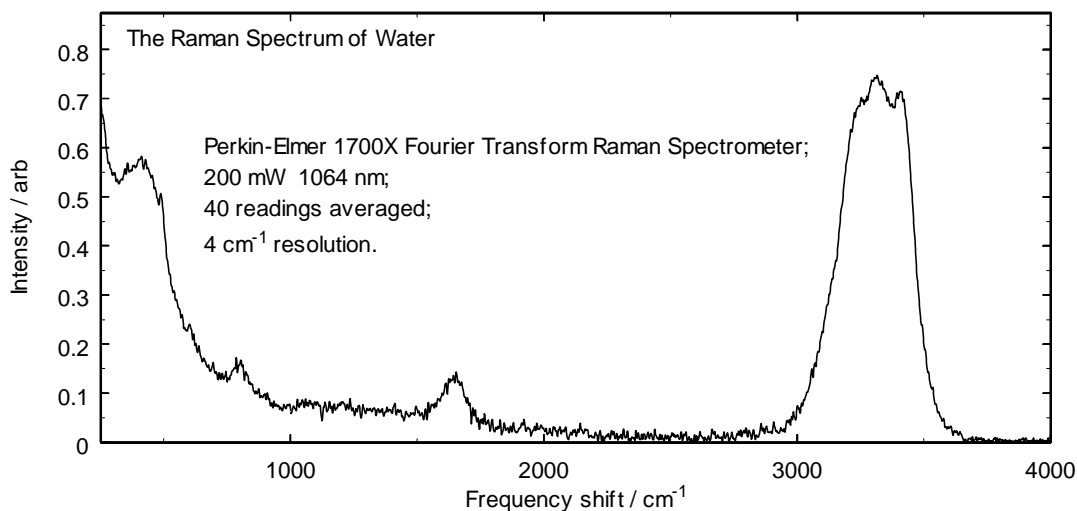


**Figure 2.4** Experimentally measured Raman spectrum of water, recorded using a commercial Fourier transform interferometer, with 1064 nm incident light from a Nd-YAG laser.

It can be seen that the bands of (hydrogen-bonded) water (figure 2.4) are much broader than those of the two non-polar solvents (figure 2.5); the rise in Raman scattering intensity towards the laser line is due to hydrogen bonding. The rising baseline in figure 2.5 is an artifact of the (dispersive) spectrometer optics, and is believed to be due to fluorescence of the optical components. The frequency shifts in figures 2.4 and 2.5 are towards lower frequencies, *ie* Stokes bands are plotted.

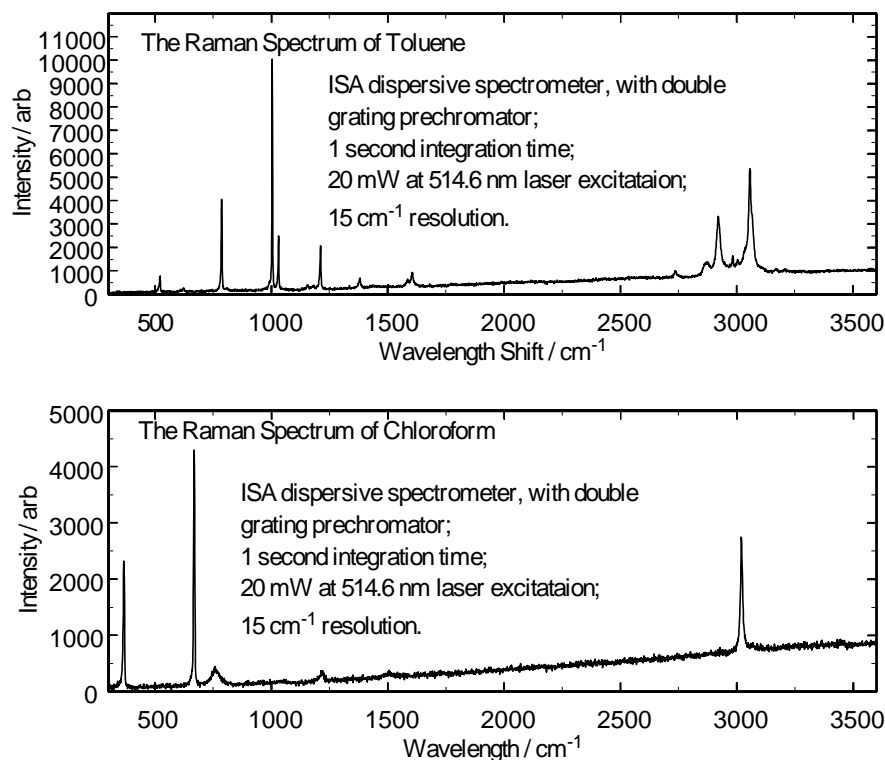


**Figure 2.5** The Raman spectra of chloroform and toluene recorded using a commercial dispersive spectrometer equipped with a CCD camera and double grating prechromator.

In comparing the spectra above, although the intensity scale of the FT device cannot be directly related to that of the dispersive spectrometer, it may be noted that the scattering cross section (integrated over its width) of the 1002 cm<sup>-1</sup> line of toluene is only 30% greater than that of the 3400 cm<sup>-1</sup> line of water<sup>[45][40]</sup>, although the peak scattering cross section of the toluene line is over an order of magnitude greater.

#### 2.2.14. The resonance Raman effect

A related phenomenon is that of *resonance Raman scattering*<sup>[39]</sup>. If progressively higher photon energies are incident on a sample, eventually the  $\nu^4$  dependance of equation 2.5 breaks down. This happens as the energy of the incident photons approaches that of the molecular electronic levels. The Raman scattering cross section may increase by  $10^6$  as the electronic energy level is approached, for instance, Hofmann and Moser<sup>[50]</sup> measured an intensity increase by a factor of 850 in the 813 cm<sup>-1</sup> line of KNO<sub>2</sub> as the incident wavelength was changed from 436 nm to 254 nm. At even shorter wavelengths Barletta and Veligdan<sup>[51]</sup> found the scattering cross section of CCl<sub>4</sub> to increase by  $1.6 \times 10^4$  with 248 nm incident light.

Although the Raman scattering cross section can rise dramatically at resonance, the scattered radiation may be concealed by a simultaneous increase in absorption, or by fluorescence emission. The effect is not beneficial to this work. By choosing a sufficiently short incident wavelength for resonant Raman scattering from a particular molecule, it is more likely that problems from fluorescence of other compounds in our analyte will be encountered. For instance, the electronic absorption spectra of toluene<sup>[52]</sup> and chloroform<sup>[53]</sup> are in the ultraviolet, and any attempt to produce Raman spectra from these in a cross-contaminated analyte will certainly suffer from fluorescence masking.

### 2.2.15. Surface enhanced Raman scattering (SERS)

Between 1974<sup>[54]</sup> and 1977<sup>[55]</sup> experiments studying the Raman scattering intensity of molecules adsorbed on to the surface of metal electrodes showed that the Raman scattering intensity of the adsorbed molecule could be increased by as much as  $10^6$  times. While, because of the problems associated with surface fouling, this surface enhancement effect has not been used in this work, it is described briefly here for completeness, and as a potential extension to what has been done. Garrell<sup>[56]</sup> has written an introduction to the subject, including analytical applications, and Chang and Furtak<sup>[57]</sup> edited a convenient introduction to the theory.

The models used to describe the origin of SERS may be broadly divided between molecular and electromagnetic descriptions. Molecular theories contend that the polarizability  $\alpha$  is enhanced, that molecules adsorbed on to a metal surface may be orientated preferentially with respect to the incident electric field and that the electronic structure of the molecule may be altered such that the incident light approaches the energy of a modified molecular resonance. Electromagnetic explanations invoke image fields in the metal substrate, electric field vector enhancements due to the shape of the substrate ('lightning rod' effects), surface plasmons, and charge transfer between the substrate and molecule. In general, both molecular and electromagnetic enhancement mechanisms both play a part in the enhancement effect, although the relative importance of the molecular and electromagnetic models varies widely from case to case.

The experimental results are remarkable, both in the magnitude of the observed enhancement, and the wide range of analytes amenable to the technique. Silver, copper, and gold are the most commonly used substrates<sup>[57]</sup>, the most universal substrate being silver. Pyridine adsorbed on to silver substrates displays an enhancement of up to  $10^6$ , approximately constant between 700 nm and 500 nm<sup>[57][58]</sup>. The enhancement varies for different adsorbates, and for each vibrational band of a molecule, and is a function of the incident wavelength. Silver substrates display a maximum

enhancement between 500 nm and 700 nm, whereas copper and gold substrates are most efficient in the near infrared (NIR)<sup>[57]</sup>.

In the laboratory, many environmentally important classes of molecule have been studied with SERS. For instance, Alak<sup>[59]</sup> has demonstrated detection of  $10^{-6}$  M concentrations of chlorinated pesticides in aqueous solution in a 4 second integration time. Storey *et al*<sup>[60]</sup> have measured chlorinated hydrocarbons *in situ* at 10 ppm in ground water, and low ppm sensitivities for benzene and naphthalene in ground water have been reported by Carron *et al*<sup>[61]</sup>. However, despite its attraction for low level measurement, the use of SERS for *in situ* analysis is effectively not a direct spectroscopy as described at the beginning of this chapter, due to the involvement of the surface layer. It requires a carefully prepared probe, which is, by the nature of the technique, susceptible to fouling.

## 2.3. Elastic Light Scattering

Fluorescent emission and Raman scattering can both be described as *inelastic* processes: the energy of the scattered photons is not conserved. The light has a different frequency (and hence a different wavelength) after the interaction, and it is this change which enables us to deduce the presence of an analyte. However, light is more commonly scattered without any change in energy: the frequency of the photons is unchanged, and the process is termed *elastic*. Elastic light scattering can be used to measure the size, density, and shape of scattering particles<sup>[62]</sup>, but in this work it can be the major source of noise in the measurement of the inelastically scattered light; to avoid inelastically scattered light, one needs to know where it is coming from, and where it is going to.

### 2.3.1. Rayleigh scattering

When light is scattered by particles that are sufficiently well spaced that the scattering from each is incoherent, and small enough that the scattered light may be considered to originate from a single point, then the scattering may be described by the theory of Rayleigh scattering. As in Raman scattering from molecules, the scattering centres behave individually as electric dipoles, and the scattering pattern has the text book dipole distribution and  $1/\lambda^4$  variation of intensity<sup>[38]</sup>. Because the scattering from each centre is unrelated to that from the next, the net irradiance at any point is simply the sum of the irradiances of each scattering centre. All matter will scatter light by this mechanism.

### 2.3.2. Mie scattering

The Mie scattering theory includes the size, shape, refractive index, and absorptivity of the scatterers, and reduces to Rayleigh scattering as a special case<sup>[38]</sup>. It should be used where the size of the scattering centres is larger than  $\lambda/10$ , *ie* when the scattering within each particle becomes the sum of the scattering from *coherently* radiating dipoles. As the size of the scattering centres increases with respect to the wavelength of the scattered light, the scattering becomes concentrated in the forward and reverse directions, and the scattering intensity becomes independent of the scattering wavelength (*ie* white light scattering). Particles of dust, water droplets, net curtains, and materials with gross random variations of refractive index will scatter light by this mechanism. For particles much larger than the wavelength of the scattered light, the macroscopic laws of refraction and Fresnel reflection apply, resulting in mainly forward scattering.

### 2.3.3. Fresnel reflections

*Fresnel reflection* is the term given to the partial reflection of light incident on a boundary between materials with different refractive indices. Fresnel reflection is a consequence of the same electromagnetic equations and boundary conditions as Mie scattering, but applied to macroscopic situations<sup>[63]</sup>. The reflectance and transmittance coefficients  $R$  and  $T$  are given for non-magnetic media by equations 2.18 and 2.19. The subscripts  $\perp$  and  $\parallel$  refer to the cases that the electric field vector is perpendicular or parallel to the *plane of incidence*<sup>1</sup> respectively,  $i$  and  $t$  are the angles of incidence and transmission with respect to the surface normal,  $n_i$  and  $n_t$  are the refractive indices of the incident and transmitting media.

$$R_{\perp} = \left( \frac{n_i \cos(i) - n_t \cos(t)}{n_i \cos(i) + n_t \cos(t)} \right)^2$$

$$T_{\perp} = \left( \frac{2n_i \cos(i)}{n_i \cos(i) + n_t \cos(t)} \right)^2$$
(2.18)

---

<sup>1</sup>The plane of incidence is the plane in which the incident, reflected, and transmitted rays all lie.

$$R_{\parallel} = \left( \frac{n_1 \cos(t) - n_t \cos(i)}{n_1 \cos(t) + n_t \cos(i)} \right)^2 \quad (2.19)$$

$$T_{\parallel} = \left( \frac{2n_1 \cos(i)}{n_1 \cos(t) + n_t \cos(i)} \right)^2$$

The angle of incidence  $i$  is related to the angle of transmission  $t$  by Snell's law, equation 2.20.

$$n_i \sin(i) = n_t \sin(t) \quad (2.20)$$

Equations 2.18 and 2.19 do not apply to films with thicknesses comparable to the coherence length of the light propagating through them; optical interference will modify the reflectance and transmittance at such an interface, *ie* in the case of anti-reflection coatings<sup>[64]</sup>.

## 2.4. Making Optical Spectroscopic Measurements

The techniques which may be used to resolve different wavelengths of light from one another, and quantify the energy in each measured spectral band, are briefly described here with their relative merits. Light intensity measurements are described in section 2.5.

### 2.4.1. Fourier transform spectrometers

This is not so much a spectroscopic arrangement, rather a generic means of processing the optical signals without a traditional monochromator to analyse the light spectrum. The method involves detection of the optical signal, via an interferometer having a scanned path-length difference. A two-path interferometer acts as an optical filter, having a periodic transmission  $T(\nu)$ , with a function of optical frequency  $\nu$  where

$$T(\nu) = 1 + \sin(k(\nu)) \quad (2.21)$$

The constant,  $k$ , depends on the optical path differences in the interferometer. When a complex light spectrum  $I(\nu)$  is passed through an interferometer onto a detector with a spectral response  $D(\nu)$ , then the detected signal is  $S(\nu)$ .  $S(\nu)$  is given by

$$S(\nu) = \int_{\nu=\nu_{\max}}^{\nu=\nu_{\min}} I(\nu) \cdot T(\nu) \cdot D(\nu) \cdot d\nu \quad (2.22)$$

The function  $S$  represents the correlation between the sinusoidal transmission function of the interferometer and the combined spectral responses of the input light spectrum and the spectral

response of the detector. Clearly, the correlation is best with spectral variations having the same (optical-frequency) periodicity as the interferometer. In the simplest case, where  $I(\nu)$  is a narrow line spectrum of constant frequency, the signal  $S$  represents a single (sample) point on the sinusoidal response. If the path-length of the interferometer is now scanned, its periodic transmission-response function will translate across the frequency band (and also change its period versus frequency). The detected signal will therefore vary, as the correlation between the spectral features and the periodic interferometer response varies. In the simplest case of the line spectrum, the detected signal will vary sinusoidally as the interferometer is swept. More complex spectra can be considered to consist of a linear addition of a series of such narrow-line spectra, each having an appropriate amplitude. For a complex spectral response, the variation of the detected signal with time, as the interferometer is swept, represents the inverse Fourier transform of the original spectrum. The spectrum can therefore be recovered by Fourier transformation of the temporal variations in detected signal, resulting when the interferometer is scanned. This is again illustrated by the simple example of the line spectrum, which results in a sinusoidal temporal response. The Fourier transform of a sinusoidal signal has a single value, corresponding to the single frequency of the line spectrum.

When compared to conventional spectrometers, the Fourier transform system has several advantages. The first is that it is relatively easy to obtain high spectral resolution by using a long 'path' difference interferometer (10 cm path difference at 1  $\mu\text{m}$  wavelength, results in a fractional resolution of around 1 part in 10,000). The second is that a significant fraction of the source light is incident on the detector at all times, because the mean transmission of the interferometer is much higher than that of a narrow band grating monochromator, thereby improving the optical efficiency. The third is that the interferometer can be designed with a large optical aperture, giving much higher optical throughput from radiance-limited optical sources. The advantages are less significant when only moderate resolution is needed and low-noise (*eg* CCD) detector arrays can be used, as these also allow parallel detection of each spectral component.

The main disadvantage is normally the need for a precisely-aligned interferometer, with its necessary thermal and mechanical stability. Fourier Transform spectroscopy is applicable to a wide variety of spectroscopic techniques, including transmission, reflectance, fluorescence and Raman spectroscopy, as, in all of these cases, it can be used for spectral analysis before the detection system.

### 2.4.2. Dispersive (grating) spectrometers

For use in this project a spectrograph based around a holographically ruled concave diffraction grating from Jobin-Yvon/ISA (section 3.2) has been designed and built. The main results relevant to its operation are presented here. For more information the reader should consult one of the many text books dealing with diffraction grating physics, such as the one written by Thorne<sup>[7]</sup>.

### 2.4.3. Diffraction grating equations

Referring to figure 2.6, the equation relating the angle of incidence  $i$  and reflection (diffraction)  $r$  for collimated light of wavelength  $\lambda$  on to a planar diffraction grating ruled with a pitch (line spacing)  $d$  is

$$m\lambda = d(\sin(i) + \sin(r)). \quad (2.23)$$

Here  $m$  is a positive or negative integer (including zero), and is referred to as the *order* of the diffracted beam. The zeroth order,  $m=0$ , represents specular reflection,  $i=-r$ . If an order is on the opposite side of the zeroth order to the incident beam then  $m$  is negative, illustrated in figure 2.6(a). The angles  $i$  and  $r$  are both measured in the same direction, with respect to the normal of the grating.

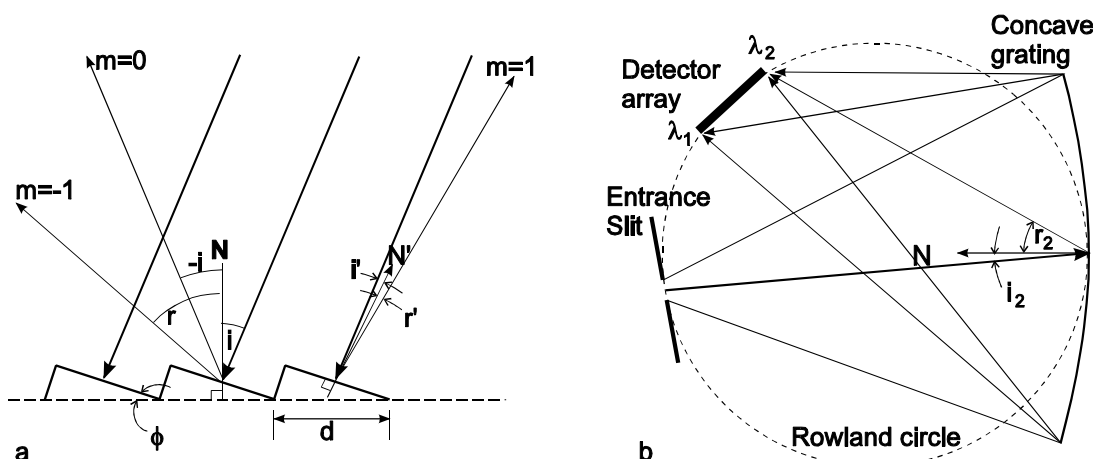


**Figure 2.6** (a) A ray diagram of light incident on to a blazed diffraction grating. (b) Using a concave grating eliminates the need for focusing optics.

The input of a spectrometer is usually a slit, and the light from this slit is collimated by lenses or mirrors in the spectrometer. These focusing optics can be eliminated through the use of a concave grating. The angle of diffraction is calculated as before, the angles  $i$  and  $r$  being measured between rays incident on to the centre of the grating and the normal to it. The configuration

illustrated in figure 2.6(b) is that of Rowland<sup>[7]</sup>, who showed that a concave grating can act as its own collimator. The entrance slit is on the *Rowland circle*, a circle with a diameter equal to the radius of curvature of the diffraction grating, and for small apertures the diffracted rays are also focused on to the Rowland circle. The particular benefit of this configuration is that the first type coma<sup>[38]</sup> of the image of the entrance slit is zero. By careful control of the groove spacing<sup>[65]</sup> other optical aberrations can be corrected too.

Evidently, from equation 2.23, light of wavelength  $\lambda$  can be diffracted at several angles ( $r$ ), corresponding to the different orders ( $m$ ). This is wasteful, and may contribute to the stray light within a spectrometer. In fact light can be directed preferentially into orders at a particular angle by blazing the diffraction grating, as illustrated for the  $m=1$  case in figure 2.6(b). In this case, the incident and refracted light are both almost along the groove normal, an arrangement known as the Littrow configuration<sup>[7][65]</sup>. In general, the diffracted light will be concentrated into any order in which light is specularly reflected from the groove surfaces; *ie*  $i'=-r'$ .

For a spectrograph, the *angular dispersion* of the grating can be found by differentiating equation 2.23, where  $i$  is a constant, to give

$$\frac{dr}{d\lambda} = \frac{m}{d \cos(r)}. \quad (2.24)$$

For a grating with focal length  $f$  the *linear dispersion* is defined as

$$\frac{d\lambda}{dx} = \frac{f}{dr/d\lambda} \quad (2.25)$$

where  $dx$  is an incremental distance across the focal plane of the detector. From the linear dispersion the wavelength incident on each part of the detector array, and the resolution of the spectrometer, may be found (assuming that diffraction at the input slit is negligible).

When perfectly monochromatic light is incident in to a spectrometer through, for instance, a slit, an image of the entrance slit is formed at the detector. The minimum dimension of the image is diffraction limited by the size of the dispersing element, assuming that the whole of the element is illuminated. For a circular diffraction grating, of diameter  $D$ , the diameter of the central portion of the diffracted image  $a$ , can be found by considering the grating as a circular aperture<sup>[38]</sup>, so

$$a = 1.22 \frac{2f\lambda}{D} \quad (2.26)$$

where  $f$  is the focal length of the spectrometer and  $\lambda$  is the wavelength of the diffracted light. If the image of the slit is larger than  $a$ , then the resolution of the spectrometer is simply determined

by the geometrical image of the entrance slit and the linear dispersion of spectrometer (assuming that the detector width is less than that of the image). For the 70 mm diameter grating used in this project the diffraction limited image size is 5.5  $\mu\text{m}$  and so the system resolution is determined by our entrance aperture, defined by fibre ends of diameter 400  $\mu\text{m}$ .

#### 2.4.4. Stray light and ghost lines

An effect which may further limit the performance of a spectrometer, especially if low intensity bands must be resolved from much higher intensity ones, is *stray light*<sup>[65]</sup>. The term encompasses all spurious light incident on to the detector, other than that at the wavelength of interest, and can be broadly divided between *randomly scattered light* and *focused stray light*. Randomly scattered light may be a result of dust or imperfections in the optical surfaces or reflections within the spectrometer housing of optically misaligned light, or light in those orders of diffraction not directed towards the output. Focused stray light arises from optical aberrations of the focusing optics in the spectrometer and re-entrant spectra.

Obviously optical misalignment can be avoided, and this includes matching the numerical aperture of the input light to that of the focusing optics of the spectrometer. The effect of other reflections can be reduced by *baffling* the spectrometer, which essentially entails erecting partitions within the spectrometer wherever possible, between potential sources of stray light, and the optical detector. Minimising or correcting for the effects of optical aberrations is a trade off between optical perfection and size and simplicity, but one should also be aware that even the best optical components are not perfectly polished, and the more optical surfaces are introduced in to the system, the greater the potential scattering from surfaces.

A related phenomenon in diffraction grating spectroscopy is that of ghosting, where periodic errors in the ruling of the grooves result in spurious maxima in the diffracted spectrum. This is a problem in 'traditionally' produced gratings, which are fabricated by mechanically ruling a diamond point back and forth across the surface of a polished blank. Any periodic variations in the groove spacing  $d$  (figure 2.6, equation 2.23) will result in ghost lines focused on to the detector.

Ghost lines are eliminated by the use of holographically produced gratings, which have no periodic ruling errors. The stray light performance of a holographically ruled diffraction gratings is typically a factor of ten better than that of a mechanically ruled grating<sup>[65]</sup>, and in addition, the ruling pattern can be optimised to correct for certain geometric aberrations as well. Even a perfect

diffraction grating will randomly scatter light though, as it is impossible to perfectly polish a surface. However, by making use of concave diffraction gratings which both collimate the incident light, and refocus diffracted light on to the detector, all other scattering surfaces can be eliminated from an optical system.

#### 2.4.5. Grating f-number and spectrograph numerical aperture

The light collecting properties of the input aperture of a spectrometer are either quoted as an f-number ( $f/\#$ ) or a numerical aperture ( $NA$ ) (figure 2.7). The two are related by equation 2.27.

$$NA = \frac{1}{2(f/\#)}. \quad (2.27)$$

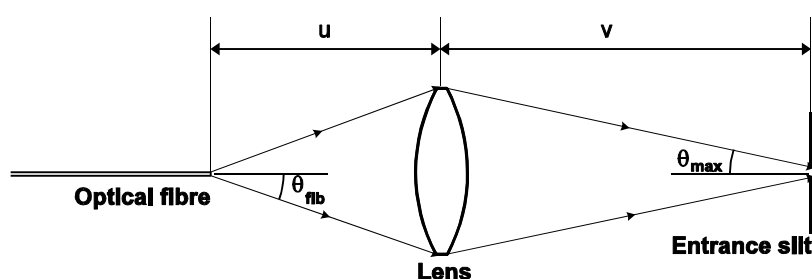


Figure 2.7 Matching the numerical aperture of a fibre to a spectrograph.

An optical fibre is also characterised by its numerical aperture, and if the numerical aperture of the fibre is greater than that of the spectrometer then the source  $NA$  must be *matched* to the acceptance  $NA$  of the spectrometer. This can be achieved with a lens of focal length  $f$  as shown in figure 2.7, where  $u$  and  $v$  are related to  $f$  by

$$u = f \left( 1 + \frac{\tan(\theta_{fib})}{\tan(\theta_{max})} \right) \quad (2.28)$$

$$v = f \left( 1 + \frac{\tan(\theta_{max})}{\tan(\theta_{fib})} \right)$$

Such matching results in a magnification of the fibre tip at the entrance slit, given (for paraxial rays) by

$$M_a = \frac{\theta_{fib}}{\theta_{max}} \quad (2.29)$$

## 2.5. Detector Technologies

The optical intensities across the output plane of the spectrograph must be converted into electronic signals to be measured. The wavelengths of light used in this work (approximately 700 nm to 900 nm) fall conveniently within the sensitive range of silicon devices<sup>[66]</sup>. Several detector configurations were investigated during the course of this work, including arrangements using discrete photodiodes, self-scanning photodiode arrays, and charge coupled device (CCD) detectors.

It was found that while discrete photodiodes in a transimpedance configuration could offer the best signal to noise measurements in theory, in practice better performance was achieved using detector array integrated circuits, such as self-scanning photodiode arrays (PDAs).

### 2.5.1. Discrete photodiodes

Photodiodes are specialised variants of the p-n junction semiconductor diode structure<sup>[66]</sup>. The doping of the device is controlled such that the junction region between the p-type and n-type material is very lightly doped (eg p- $\pi$ -n), or not doped at all (p-i-n), so that the depletion region of the device is large, and well defined, under reverse bias. Photons that are absorbed by the material within, or close to, the depletion region generate electron hole pairs, which are swept apart by the electric field gradient in the depletion region. This generates an electric current, which is detected by an external electronic circuit. Except in the rare case of multiple-photon absorption, only photons of energy greater than the characteristic band gap of the semiconductor material will be absorbed, which for silicon devices corresponds to photons of wavelength 1100 nm or shorter.

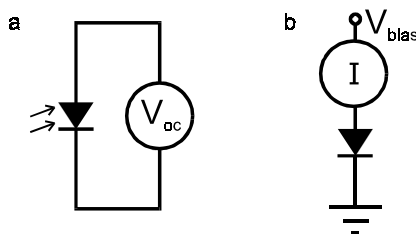


**Figure 2.8** a) A photodiode in the photovoltaic mode: the open circuit voltage across the device terminals is measured. b) In the photoamperic mode the current through the device is measured, and the voltage across the terminals is kept constant at zero, or a negative value.

Photodiodes are used in one of two modes of operation<sup>[66]</sup>: in the *photovoltaic mode*, where the photodiode is connected across the high impedance terminals of a voltage measuring circuit; or

in the photoamperic mode, where the terminals of the photodiode are kept at a constant voltage, and current generated by the device is measured using a low impedance current measuring circuit (figure 2.8). In the photovoltaic mode the output voltage is related to the incident light intensity<sup>[66]</sup> by equation 2.30.

$$V_{oc} = \frac{kT}{q} \ln \left( \frac{I_{ph}}{I_0} + 1 \right) \quad (2.30)$$

$V_{oc}$  is the open circuit voltage across the photodiode,  $k$  is Boltzmann's constant,  $T$  is the absolute temperature,  $q$  is the electronic charge,  $I_0$  is the small reverse saturation current of Shockley's ideal diode equation<sup>[66]</sup>, and  $I_{ph}$  is the photocurrent generated in the device, which is proportional to the intensity of the light falling onto the device.

As well as being non-linear, the voltage across a photodiode in the photovoltaic mode is low pass filtered by the device shunt resistance and capacitance, both functions of the voltage across the diode, and ill-defined parameters. The photoamperic configuration is much better suited to precise measurements of light intensity. In this case the closed circuit current  $I_{cc}$  is related to the photocurrent by equation 2.31, where  $V_b$  is the reverse bias voltage across the diode.

$$I = I_0 \left( \exp \left( \frac{-qV_b}{kT} \right) - 1 \right) - I_{ph} \quad (2.31)$$

The current  $I$  is usually measured in an active transimpedance configuration, such as that shown in figure 2.9, and the voltage output of the circuit can be linear of several orders of magnitude. For low frequency measurements, it is preferable to use zero reverse bias; then the reverse leakage current term  $I_0$  disappears. Although  $I_0$  is typically very small, and is often neglected, the reverse leakage current and its associated shot noise can be the dominant noise source if the incident light level is low. If the photodiode is to be used to measure rapidly varying signals then it is usually desirable to reverse bias it by a few volts. This maximises the device quantum efficiency by maximising the width of the depletion region, and increases the speed of operation of the device by reducing the junction capacitance.

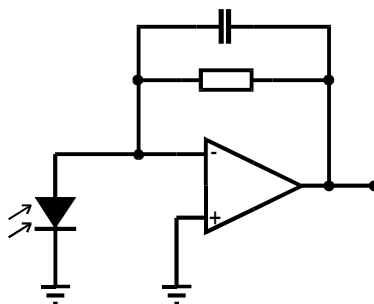


**Figure 2.9** An active transimpedance amplifier circuit: because the terminals of the photodiode are both held at the same potential, the voltage output of the circuit remains linear with respect to the incident light intensity over many orders of magnitude. The capacitor is present to maintain stability and reduce the voltage noise bandwidth.

In this work optimum signal to noise ratio was required, and so the photodiode was operated unbiased. Photodiodes with low shunt capacitance lower the voltage noise gain, and may increase the circuit bandwidth. Loop capacitance may be necessary to stabilise the circuit. The operational amplifier should have an FET input stage, as the input bias currents are the dominant noise source for large transimpedance values. The other contribution to the output noise is Johnson (or thermal) noise from the feedback resistor (the value of which defines the transimpedance in this simple circuit), and the photodiode resistance. Johnson noise is an unavoidable consequence of the second law of thermodynamics, and it experiences the same gain in the circuit of through the circuit of figure 2.9 as the photocurrent. However, it can be shown that as long as the photocurrent produces more than 51.2 mV at the output, the shot noise of the photocurrent is greater than the thermal noise of the resistor. The noise performance of a photodiode is typically specified as a noise equivalent power (NEP), which is defined as the optical power input to the system which produces an output equal to that from the noise. As an example, the NEP of one photodiode in the Hamamatsu S3954 discrete photodiode array is quoted as  $4 \times 10^{-15} \text{ W/Hz}^{1/2}$ .

Several prototype circuits were built for this work and investigated for suitability. Transimpedances of up to  $10 \text{ G}\Omega$  were studied, and the results of this worked are summarised here: circuits with large transimpedance, above  $100 \text{ M}\Omega$  become microphonic; the resistors available add considerably to the measurement noise, especially at low frequency; and large transimpedances are not useful in the event that there is any optical background in the measurement, as the amplifier will saturate. In addition the circuit complexity is proportional to the number of optical elements in any array.

### 2.5.2. Self-scanning photodiode arrays

In a self-scanning photodiode array a linear array of photodiodes is built into the same integrated circuit as the electronics required to sequentially read the voltage from each one, as shown in figure 2.10. Light incident onto the photodiodes creates electron-hole pairs by the same mechanism as for discrete photodiodes, but due to the FET switch, this charge is not free to flow immediately into an external circuit, and instead is integrated on the capacitance of the photodiode itself. The accumulated charge on each photodiode in turn is output on the video line (figure 2.10) by opening the FET switches individually.

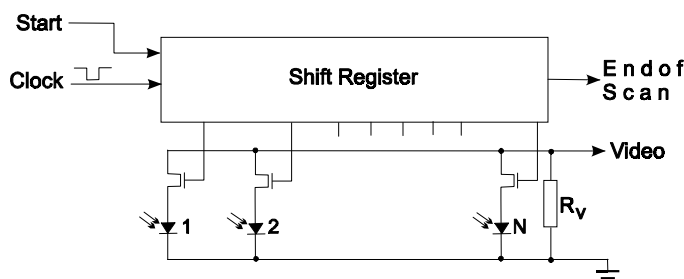


**Figure 2.10** A schematic showing the sequential readout of a self-scanning photodiode array via FET switches.

Usually the only signals that need be provided to the array are a regular clock signal and a start pulse to trigger the readout cycle at the end of each integration. Errors in the output voltage are due to integration of switching transients, thermal current, and leakage current, as well as the shot noise in the full-well charge, the thermal noise of the resistors, and noise due to any readout electronics employed (accentuated by the high capacitance on the video line). The former errors are minimised in devices which use differential output of a set of active photodiodes, and a set of dummy photodiodes, identical in construction to the active diodes, but unexposed to the light. The performance of such a device offers little room for user optimisation, except in the choice of readout electronics.

The devices are not typically cooled, and the maximum achievable signal to noise ratio decreases with longer integration times due to the depletion of the stored charge by thermally excited electron-hole pairs in the photodiodes. The device quantum efficiency is similar to that of discrete silicon photodiodes. These devices have primarily found application in optical scanners, but they are migrating into spectroscopic applications, with some devices designed specifically for spectroscopy. The NEP power for each  $25\ \mu\text{m} \times 250\ \mu\text{m}$  pixel in the EG&G Reticon self-scanning array, output through the optimum output circuitry as described in the product data sheet, was calculated from a 20 second measurement to be  $3.6 \times 10^{-15}\ \text{W/Hz}^{1/2}$ . This is smaller than that of the discrete photodiode example given in section 2.5.1 due to the smaller size of the diode; if the

output from 144 such pixels is summed, so that the area is equal to that of the diode of section 2.5.1, then the NEP is  $4.3 \times 10^{-14} \text{ W/Hz}^{1/2}$ .

### 2.5.3. Charge coupled device detectors

Charge coupled device (CCD) optical detectors are formed from (usually two dimensional) arrays of metal-insulator-semiconductor capacitors, linked so that the charge stored in each one may be transferred to adjacent capacitors by the correct sequence of bias signals. Charge is created in each capacitor when photons are absorbed in the semiconductor region of the device, which creates an electron-hole pair. The electron-hole pair is swept apart by the internal electric field, and the charge is trapped in the capacitor. The trapped charge can be measured by transferring it to the array output node.

Two distinct types of CCD detectors are made, named according to the process by which charge is transferred to the output: inter-line transfer (ILT), where the charge is transferred via lines of optically-inactive capacitors between each optically-active line; and full-frame transfer (FFT), where the charge is transferred through the optically-active capacitors. For spectroscopic work FFT devices are preferred, as the whole of the device area is optically active. ILT devices are used in video cameras, where interference between one frame and the next must be avoided.

In spectroscopic applications CCDs are usually operated cooled, either by thermo-electric Peltier coolers, or by liquid nitrogen, so that long integration times are possible free relatively from the build up of thermally excited charge. The quantum efficiency of CCD detectors is typically lower than photodiodes, and the dynamic range is lower; however, lower noise readout electronics is possible than for multiplexed photodiode arrays, and when operated at low temperature, they are the preferred option for detecting low light levels.

Using a 2D CCD it is possible to obtain several independent spectra from individual inputs to the spectrograph, *eg* separate optical fibres. This can be useful to make instantaneous calibrations against a reference sample for instance. When the input to the spectrograph is via a single entrance slit, then it is preferable to combine the charge stored in all the pixels of each column, in a process termed *binning*, so that the output of the device is identical to a linear detector array. Charge binning increases the signal to noise ratio of the measurement, and is preferable to external data averaging when the device readout noise is significant<sup>[67]</sup>. Based on measured values of the thermally accumulated charge and spectral response, the NEP of the Hamamatsu C5809-0907 CCD used in this work was  $1.3 \times 10^{-17} \text{ W/Hz}^{1/2}$  for each individual pixel,  $5 \times 10^{-16} \text{ W/Hz}^{1/2}$  for

a binned pixel of area equal to the diode of section 2.5.1. (The full data sheet of this Hamamatsu detector is reproduced in appendix C, and further details are given in section 3.5.)

The dynamic range of the CCD is limited by the full well saturation, the number of electrons that can be stored in each capacitor. There are separate limits for the individual optically-active elements, and for the end of line capacitor, which must hold all the charge from a line of capacitors.

#### 2.5.4. Electronic interference

As with all low-signal-level analogue circuitry, care must be taken in the design of optical detector circuits to shield the measured electrical signals from any potentially interfering signals from other sources. Such interference may enter the system from power supply connections, circuit interconnections, or signal interconnections between equipment. In this work, with low signal frequencies (*below 1 MHz*), interference is coupled into signal paths either by capacitive or inductive coupling; it is minimised by shielding and correct electrical grounding, as described in the following paragraphs<sup>[68]</sup>.

Interference from the power supply connections can be reduced by using high-frequency bypass capacitors in conjunction with electrolytic capacitors at the supply pins of each IC used. To prevent capacitive coupling of voltages near to the signal path, the path should be kept as small as possible. Where signals are transmitted between equipment or separate circuits, a conducting shield should enclose both signal wires, and the shield should be connected to ground at one end only<sup>[68]</sup>.

The grounding configuration of a circuit can introduce interference by two mechanisms: ground loops, and large currents flowing in ground return paths<sup>[69]</sup>. A ground loop is formed when more than one path to ground is possible. This configuration forms a loop around which current can flow, and any varying magnetic field which intersects it will induce current to flow around the loop. Also, it is unlikely that any two connections to ground will be at the same potential (for reasons outlined in the next paragraph), and this potential difference will also impress itself onto the measured signal. This can be avoided by using measuring devices with differential inputs: in this way ground loops are avoided, and any other common mode interference at the input to the measuring circuit is rejected.

When current flows to ground through a return path of finite resistance there will be a potential difference between any two points on it. If parts of a circuit that require high currents share the same ground return path as the signal voltages, then a voltage is impressed onto the signal voltage. This problem is avoided by using separate ground return paths for digital, analogue, and high current portions of a circuit. These ground paths should be connected together at only one point in the circuit, as close to the electrical supply as possible.

The same care to avoid electrical interference was taken for each of the detection techniques described in the previous sections of this chapter. In this way electrical interference was kept to a minimum, and in most experiments it was the shot noise of each measurement that was the dominant source of error.

## **2.6. Conclusions**

The techniques applicable to the quantitative and qualitative study of liquids over optical fibres have been outlined in this chapter. In this work emission techniques have been chosen over absorption techniques due to ease of probe construction (single point measurements are possible), and the possibility of making non-contact measurements. Most of the work described in the following chapters has been with fluorescent compounds, but the equipment built has been optimised for Raman spectroscopy because of the specificity of this technique, and compatibility with measuring aqueous solutions.

A dispersive spectrograph was designed and built during this work: a dispersive design was chosen for its mechanical simplicity, as the aim of the work was to build compact portable instrumentation. A Fourier transform spectrometer, while having certain advantages in a laboratory setting, was not suitable for this goal. To make optimum use of a dispersive spectrometer it is vital to make use of 'the multiplex advantage' (the possibility of measuring light intensity at many wavelengths simultaneously), so an array detector was used. Arrays of discrete photodiodes, self-scanning arrays, and CCD detectors were all investigated during this work. For optimum compatibility with vertical arrays of fibre, low noise measurement, and low circuit complexity, a CCD detector was interfaced to the spectrograph.

All the equipment used, designed, and built during this project is described in the next chapter.